Copyright © 2009 Tech Science Press CMES, vol.42, no.2, pp.131-148, 2009

High-Fidelity Tetrahedral Mesh Generation from Medical Imaging Data for Fluid-Structure Interaction Analysis of Cerebral Aneurysms

Yongjie Zhang[1], Wenyan Wang[1], Xinghua Liang[1], Yuri Bazilevs[2], Ming-Chen Hsu[2], Trond Kvamsdal[3], Reidar Brekken[4] and Jørgen Isaksen[5]

Abstract: This paper describes a comprehensive and high-fidelity finite element meshing approach for patient-specific arterial geometries from medical imaging data, with emphasis on cerebral aneurysm configurations. The meshes contain both the blood volume and solid arterial wall, and are compatible at the fluid-solid interface. There are four main stages for this meshing method: 1) Image segmentation and geometric model construction; 2) Tetrahedral mesh generation for the fluid volume using the octree-based method; 3) Mesh quality improvement stage, in which edge-contraction, pillowing, optimization, geometric flow smoothing, and mesh cutting are applied to the fluid mesh; and 4) Mesh generation for the blood vessel wall based on the boundary layer generation technique. The constructed meshes are extensively employed in a fully-coupled fluid-structure interaction analysis of vascular blood flow. This paper presents several case studies of hemodynamics in patient-specific cerebral aneurysms.

Keywords: Tetrahedral meshing, fluid-structure interaction, cerebral aneurysm.

1 Introduction

Nowadays approximately 3-6% of the population is estimated to have unruptured cerebral aneurysms [Rinkel, Djibuti, and Algra (1998)]. Since research on the specific risk for rupture has no clear conclusion yet, clinical decision-making is largely based on epidemiological studies of risk factors for subarachnoid hemorrhage. These studies identify three important factors for aneurysm formation

[1] Department of Mechanical Engineering, Carnegie Mellon University, USA
[2] Department of Structural Engineering, University of California - San Diego, USA
[3] Department of Applied Mathematics, SINTEF Information and Communication Technology, Trondheim, Norway
[4] Department of Medical Technology, SINTEF Health Research, Trondheim, Norway
[5] Department of Neurosurgery, University Hospital of North Norway, Tromsø, Norway

and rupture: hypertension, smoking, and family history [Isaksen, Egge, Waterloo, Romner, and Ingebrigtsen (2002)]. Further evidence suggests that the risk for rupture increases for aneurysms that are large in size and have a small neck/fundus ratio [Uiije, Tamano, Sasaki, and Hori (2001)].

Aneurysms rupture when tension inside the arterial wall exceeds the strength of arterial tissue. This suggests that, given the appropriate solid model for the aneurysm wall, wall tension can be reasonably estimated using numerical simulation [Isaksen, Bazilevs, Kvamsdal, Zhang, Kaspersen, Waterloo, Romner, and Ingebrigtsen (2008)]. Furthermore, computational methods can be used to estimate the effect of variability in the material parameters, wall thickness, and blood flow rates on the distribution and peaks of maximum wall tension. In order to do so accurately, a coupled fluid-structural simulation that accounts for the interaction between blood flow and movement of the arterial wall should be employed. This, in turn, necessitates the development of advanced mesh generation techniques that produce quality meshes of the fluid and solid subdomains. For proper discretization of the fluid domain there is a need for a refined mesh in a layer near the arterial walls. This boundary layer mesh is generally needed for proper estimation of the fluid flow and in particular for accurate prediction of surface tractions acting on the wall, i.e. normal stresses and shear stresses. These tractions are important for proper prediction of the arterial wall response. In addition the wall shear stresses are important for the arterial wall cell structure and influence the growth of aneurysms.

However, generating three-dimensional fluid-structure meshes directly from medical imaging data, like Computed Tomography (CT) and Magnetic Resonance Imaging (MRI), still remains a challenge. In this work we have designed a set of comprehensive procedures, which allow us to generate high-fidelity finite element meshes of patient-specific arterial geometries from volumetric imaging data. The unique feature of our approach is that the meshes contain both the blood volume and solid arterial wall. This is in contrast to just the blood volume meshes, which preclude the analyst from using three-dimensional solids to describe the arterial wall. The meshes are compatible at the fluid-solid interface, which, in principle, is not necessary, yet significantly simplifies analysis. Our meshing approach consists of four main stages:

- Image processing - Semi-automatic image segmentation was applied for identifying and segmenting the aneurysm geometry from three dimensional (3D) computed tomography angiography (CTA) images.

- Tetrahedral mesh generation for the fluid volume - We choose the octree-based isocontouring method to construct tetrahedral meshes for the fluid volume from medical imaging data.

- Mesh quality improvement - The mesh quality from the first two stages may not be good enough for finite element simulations, therefore post-processing techniques are adopted to improve the mesh quality, including edge contraction, optimization, pillowing, smoothing and mesh cutting.
- Mesh generation for the blood vessel wall - Given the mesh from the previous stage, a boundary layer generation technique is utilized to construct meshes for the blood vessel wall.

The remainder of this paper is organized as follows: Section 2 reviews the related work on mesh generation and blood flow simulation. The detailed mesh generation algorithm is described in Section 3. Section 4 briefly describes the fluid-structure analysis procedures employed in the simulation of cerebral aneurysms. Section 5 shows the meshing and simulation results for four aneurysm models. Conclusion and future work are given in Section 6.

2 Previous Work

Tetrahedral Mesh Generation: Octree-based, advancing-front-based and Delaunay like techniques were widely used for tetrahedral mesh generation. For the octree-based technique, the cube containing the geometric model is recursively subdivided until the desired resolution is reached [Shephard and Georges (1991)]. Advancing front methods begin from a boundary and move a front from the boundary towards the empty space within the domain [Lohner and Parikh (1988)]. The Delaunay criterion guarantees that no node is contained within the circumsphere of any tetrahedra of the mesh, which is called "empty sphere". The triangles or tetrahedra are refined locally by inserting new nodes to maintain the Delaunay criterion. Various techniques were investigated to define new nodes [Chew (1997)]. Sliver exudation [Cheng, Dey, Edelsbrunner, Facello, and Teng (2000)] was developed to remove these slivers. A deterministic algorithm [Cheng and Dey (2002)] was presented to generate a weighted Delaunay mesh without poor quality tetrahedra including slivers. Shewchuk (2002) solved the problem of enforcing boundary conformity by constrained Delaunay triangulation (CDT).

Because many 3D objects are sampled in volumetric data, Fujishiro, Y. Maeda, and Takeshima (1996) extended the Marching Cubes algorithm (MC) [Lorensen and Cline (1987)] to extract tetrahedral meshes between two isosurfaces directly from volume data. The extraction process was accelerated by using a Branch-on-Need octree as an auxiliary data structure. Marching Tetrahedra (MT) was proposed for interval volume tetrahedralization [Nielson and Sung (1997)] as a different algorithm. Zhou, Chen, and Kaufman (1997) generated a multi-resolution framework by combining recursive subdivision and edge-bisection methods.

Quality Improvement: There are three categories of algorithms for mesh improvement [Owen (1998)]: local coarsening/refinement by deleting/ inserting points, local remeshing by face/edge swapping, and mesh smoothing by relocating vertices. Laplacian smoothing, in its simplest form, relocates the vertex position at the average of its neighbor nodes. Although Laplacian smoothing generally works well for meshes in convex regions, it may produce distorted or even inverted elements near concavities in the mesh. In order to avoid the creation of inverted elements, Field (1988) constrained the node movement. The contribution of each neighboring node in the average function was considered in [George and Borouchaki (1998)]. The Laplacian operator was discretized by using Voronoi cells and the mixed Finite Element/Finite Volume method [Meyer, Desbrun, Schroder, and Burr (2002)]. Using the finite difference method [Xu, Pan, and Bajaj (2003)], the discretized format was able to solve surface modeling problems. Hansbo (1995) developed methods which extend to anisotropic meshes. Furthermore, people searched an optimization technique to improve the mesh quality instead of relocating vertices based on a heuristic algorithm. The optimization algorithm measures and attempts to optimize the quality of the surrounding elements to a node, which is similar to a minimax technique used to solve the circuit design problem [Charalambous and Conn (1978)]. The optimization-based smoothing yields better results but is more expensive than Laplacian smoothing. Therefore, a combined Laplacian and optimization-based approach was recommended in [Canann, Tristano, and Staten (1998)], which generally uses Laplacian smoothing and only uses optimization-based smoothing when necessary.

Boundary Layer Generation: Techniques for generating boundary layers can be classified into two categories: Eulerian methods and Lagrangian methods. Eulerian methods describe the interface using an explicit surface representation such as level set methods [Osher and Fedkiw (2003)], volume-of-fluid methods [Harvie and Fletcher (2000)] and phase-field methods [Chen (2002)]. They have been widely used for their simplicity and robustness, but the accuracy may be low if there are singularities and topological changes. Lagrangian methods trace the interface using an implicit representation, e.g. marker particle [Rider and Kothe (1995)] and front tracking methods [Glimm, Grove, Li, and Tan (2000)]. They generally offer higher accuracy at lower cost and perform better than implicit representations. However, existing Lagrangian techniques often suffer from growing oscillations or self-intersections [Sethian (1999)].

Blood Flow Simulation: Simplified geometries were adopted in initial attempts to simulate blood flow in arteries. This approach was restricted because it is unable to represent complex flow phenomena in real blood vessels. Taylor, Hughes, and Zarins (1998) first used real-life geometries to simulate blood flow, and established

the concept of patient-specific cardiovascular modeling, which opened the door for designing predictive tools of vascular modeling and treatment planning. Although dramatic improvements in the computational results were obtained in [Taylor, Hughes, and Zarins (1998)], the blood vessel wall was assumed to be rigid. However, the flexible and rigid wall computations [Torii, Oshima, Kobayashi, Takagi, and Tezduyar (2006)] indicated that the rigid wall assumption precludes pressure wave propagation and overestimates wall shear stress. While several methods can be used to include the effect of the moving wall in computations, the arbitrary Lagrangian-Eulerian (ALE) approach was the most prevalent [Farhat and Geuzaine (2004)]. Applications of ALE to hemodynamics were discussed in [Formaggia, Gerbeau, Nobile, and Quarteroni (2001)]. The other techniques partially include the coupled momentum method [Figueroa, Vignon-Clementel, Jansen, Hughes, and Taylor (2006)], the immersed finite element method [Liu, Liu, Farrell, Zhang, Wang, Fukui, Patankar, Zhang, Bajaj, Lee, Hong, Chen, and Hsu (2006)], and the space-time finite element method [Tezduyar (2003)].

3 Meshing Algorithm

There are four main steps in our mesh generation algorithm starting from the input patient-specific imaging data: data acquisition and image processing, octree-based tetrahedral meshing for fluid volume, quality improvement, and boundary layer generation.

3.1 Data Acquisition and Image Processing

The 16 bit CTA data sets are RAW images with a size of 512x512xN. N represents the number of images in the DICOM series, which in this case equals to the number of images acquired in the axial direction. A lot of image processing techniques, especially segmentation, have been developed and applied to medical imaging data [Goncalves, Tavares, and Jorge (2008); Zhang, Cheng, Oh, Spehar, and Burgess (2008); Yang, Tang, Yuan, Kerwin, Liu, Canton, Hatsukami, and Atluri (2008)]. In our study, the RAW image data volume was loaded into the open source application ITK-SNAP which includes a level-set implementation of active contour segmentation [Yushkevich, Piven, Hazlett, Smith, Ho, Gee, and Gerig (2006)]. A region of interest containing the aneurysm and the connecting vessels was manually identified, and several seed points for the segmentation were set inside the aneurysm. The seed points were inflated until they reached a region of different image intensity, and eventually grew together into one shape filling the aneurysm and connecting vessels. All the segmented models were visually evaluated, and in some cases manual corrections were made to obtain satisfying results. The geometries were exported as StereoLithography (STL) files used as input for the mesh

generation.

3.2 Octree-Based Tetrahedral Meshing for Fluid Volume

The tetrahedral meshing method in this paper is based on a top-down octree subdivision and isocontouring method [Zhang, Bajaj, and Sohn (2005)]. We aim to construct crack-free, self-intersection free, no hanging nodes, and valid tetrahedral meshes from imaging data. For each octree cell, we calculate a minimizer point using a Quadratic Error Function:

$$QEF(\vec{x}) = \sum_i [\vec{n}_i \cdot (\vec{x} - \vec{p}_i)]^2, \tag{1}$$

where p_i, n_i are the position and unit normal vectors of the interaction points. Here we analyze two kinds of edges: the sign change edge with two endpoints on different sides of the isosurface, and the interior edge with two endpoints inside the fluid volume. In the uniform case, both of them are shared by four cells, and we calculate one minimizer point for each of them. For each sign change edge, we connect the four obtained minimizer points and its interior endpoint to construct a pyramid as shown in Fig. 1(a). Similarly as shown in Fig. 1(b), we obtain a diamond for each interior edge. In the adaptive case, the sign change edge or the interior edge is shared by either four or three cells. Therefore, we obtain four or three minimizer points. A pyramid or a tetrahedron is constructed for a sign change edge, and a diamond or two tetrahedra are constructed for an interior edge. The next step is to split the pyramid or diamond into tetrahedra.

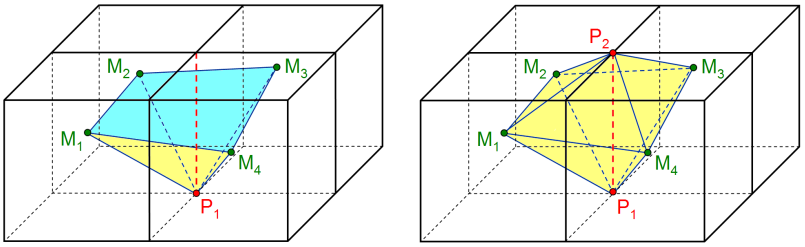

(a) (b)

Figure 1: (a) A pyramid formed by analyzing the sign change edge; (b) a diamond formed by analyzing the interior edge.

There are two ways to split a pyramid into tetrahedra by choosing different diagonals. In this paper, for the aim of generating good quality meshes without self-intersection, if the quadrilateral formed by the four minimizer points is concave,

the diagonal containing the concave point is used to split the pyramid. Otherwise, we compare the aspect ratios and choose the diagonal which gives us better aspect ratio. Splitting a diamond to tetrahedra also has two ways. As shown in Fig. 2(a), one is to choose a diagonal of the quadrilateral, similar to the pyramid case, split the quadrilateral into two triangles, and then connect the two triangles with the two endpoints of the analyzed edge. The other way is to connect the two endpoints and each pair of adjacent minimizer points as shown in Fig. 2(b). Both ways generate four tetrahedra for each interior edge, but the second way turns out to be better due to its robustness. Ideally, the two endpoints of an interior edge are on the different sides of the obtained triangles. However, there are some special cases that they are on the same side. The second method not only works in all the possible cases, but also outperforms the first one even when it is valid. For a typical case that all the four minimizer points are in the center of the each cell, the worst edge ratio using the first method is $\sqrt{2}$ while the worst edge ratio using the second method is $\frac{2}{\sqrt{3}}$ (the edge ratio here is the ratio of the longest edge to the shortest edge). Therefore the second method is adopted to split the diamond.

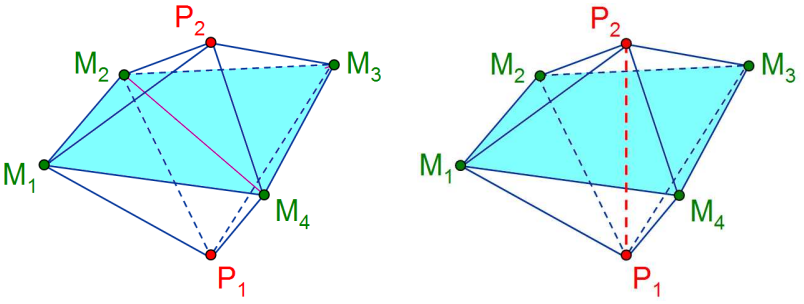

(a) (b)

Figure 2: (a) Splitting a diamond into four tetrahedra by the first way; (b) Splitting a diamond by the second way.

3.3 Quality Improvement

We choose the edge-ratio, Joe-Liu parameter [Liu and Joe (1994)], and minimum volume bound as criteria to measure the quality of constructed tetrahedral meshes. The edge-ratio of a tetrahedron is the length ratio of the longest edge over the shortest edge. The definition of Joe-Liu parameter is

$$Joe-Liu\ parameter = \frac{2^{2(1-\frac{1}{d})} \times 3^{\frac{d-1}{2}} \times \mid s \mid^{\frac{2}{d}}}{\Sigma_{0\le i<j\le 3} \mid e_{ij} \mid^2}, \tag{2}$$

where d is the space dimension ($d = 3$ for a tetrahedral), $\mid s \mid$ denotes the element volume, and $\mid e_{ij} \mid$ are the lengths of the edges connecting vertices i to j. Poor quality meshes may lead to poorly conditioned stiffness matrices and make the following analysis difficult, therefore edge contraction, pillowing, and smoothing are used to improve the quality of the constructed tetrahedral meshes for the fluid volume.

3.3.1 Edge Contraction

Edge contraction is used to remove the non-manifold situation. For example, the mesh may have some non-manifolds where more than two boundary triangles share the same edge on the surface. Since the following steps like boundary layer generation and pillowing can not handle the non-manifold mesh, we have to use the edge contraction approach to remove them. Contracting an edge is the operation that removes an edge and simultaneously merges its two endpoints. For tetrahedral meshes, there are two cases which we should pay attention to: (1) if the edge has only one vertex lying on the boundary, we should only merge the edge to the boundary endpoint; and (2) if the edge has one endpoint with the valence number four, we should remove all the elements sharing this vertex before the edge contraction operation is carried out.

3.3.2 Pillowing

Mesh quality improvement will be limited if all the four vertices of one tetrahedron are on the surface, or three vertices of one triangle are on the surface but the triangle is inside the volume. The pillowing technique can eliminate these two situations by generating a new surface parallel to the original one. Vertices used to be on the original surface are now inside the mesh and can be freely moved. For each triangle $V_1V_2V_3$ on the boundary surface, a duplicated triangle $V_1'V_2'V_3'$ is constructed. These two triangles form a prism $V_1V_2V_3 - V_1'V_2'V_3'$. Then we split the prism into three tetrahedra. To avoid the diagonal conflict problem, we always split the prisms by connecting the diagonal from the smallest vertex index in the triangle $V_1V_2V_3$ to the largest vertex number in the triangle $V_1'V_2'V_3'$.

3.3.3 Optimization-Based Geometric Flow Smoothing

We choose the optimization-based smoothing to improve the worst element of the mesh, and use the geometric flow smoothing [Zhang, Xu, and Bajaj (2006)] to improve the overall mesh quality. Sometimes the two methods are used alternately. In optimization, the Laplacian smoothing operation is used to improve the minimum volume bound of the mesh, which measures the minimum volume of all elements surrounding a node. To avoid inverted elements or elements with negative

volume, we use a "smart" Laplacian smoothing operation which relocates points only if the minimum volume of the local mesh is improved. In the geometric flow smoothing, the interior vertex is moved towards the mass center using its neighboring elements. For each boundary vertex, we calculate the mass center using its neighboring boundary triangles, and then project the mass center onto its tangent plane. In this way the surface feature is preserved, and the overall aspect ratio of the mesh is significantly improved. However, this method is heuristic and may introduce invalid elements. Therefore we add one constraint: for each relocation we will keep the original position if the movement makes the neighboring minimum volume worse.

3.3.4 Mesh Cutting

The aneurysm model has both inlets and outlets. Due to the request from the fluid-structure interaction (FSI) simulation, all the vertices on each inlet/outlet have to be coplanar. Hence in this step we use one plane to cut the inlet/outlet branch to make sure that all the vertices are coplanar. We first calculate the center, the average normal direction and the radius for each inlet/outlet surface, then use the center and the average normal to define the cutting plane. There are five cases to cut one tetrahedron using a plane. In Fig. 3(a), since all the four vertices are outside of the cutting plane, all we have to do is to simply delete this element. In Fig. 3(b), because there is only one vertex inside the fluid volume, we calculate the three intersection points and connect them with the interior vertex. In Fig. 3(c), the tetrahedron has two vertices inside the fluid volume, so we calculate the intersection points and split the two quadrilaterals using the diagonal containing the smaller index. In Fig. 3(d), the tetrahedron has three vertices inside the fluid volume, and similarly we split the three quadrilaterals as in Fig. 3(c). The last case (Fig. 3(e)) is with all the four vertices inside the fluid volume, so we just keep this element. Generally, mesh cutting makes the mesh quality around the inlet/outlet plane worse. Therefore after cutting, we have to improve the mesh quality again especially for the region around the inlet/outlet. We add two additional constraints to the smoothing: the vertices on the boundary curve of the inlet/outlet plane are restricted to move along the curve, and the vertices inside the plane can only move on that plane.

3.4 Boundary Layer Generation

The blood vessel wall of the aneurysms is constructed by growing one or more boundary layers based on the fluid mesh. Suppose the boundary layer thickness is t, and we want to construct n boundary layers. We begin by duplicating all the triangles on the surfaces that need to generate a boundary layer, which creates two identical overlapping faces. The original one will provide the surface mesh on the

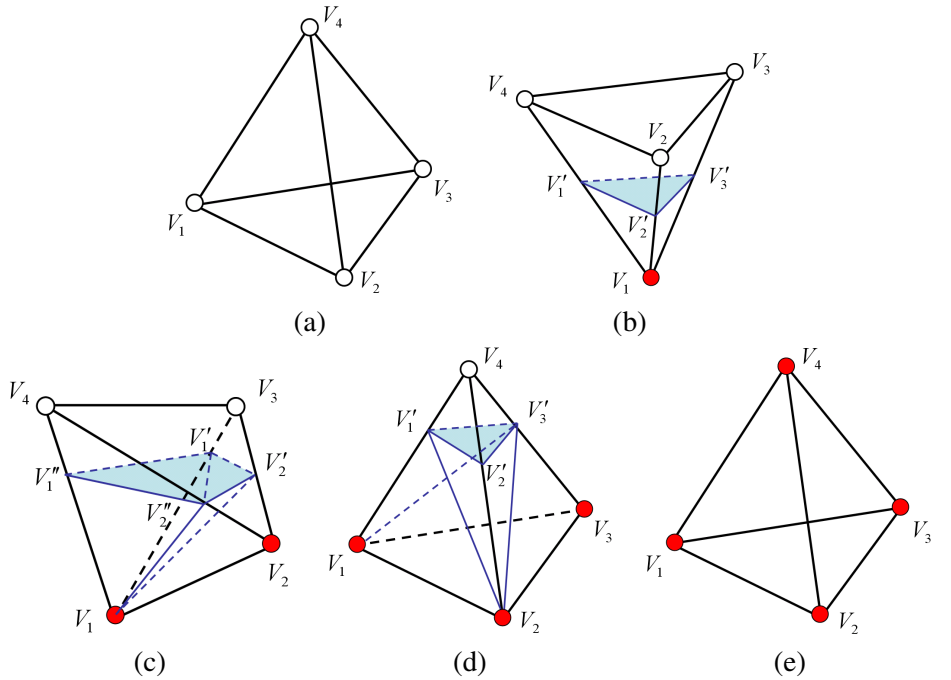

Figure 3: Five cases for cutting a tetrahedron using a plane. (a)-(e) show the case with zero, one, two, three, and four vertices inside the fluid volume, respectively.

model boundary, and the duplicated one is then relocated by moving each vertex along the normal direction for a distance t. The new boundary layer mesh is formed after connecting the original vertex to the duplicated one. After the first step, the original and duplicated triangles define a prism. Each prism will then be subdivided into three tetrahedra, which is similar to the procedures in pillowing. If all of the newly generated tetrahedra are in good quality, the boundary layer generation is done. However, if the vertices are near sharp corners or the cutting planes, the normal may intersect with its neighbors. In this case, the generated tetrahedra may intersect with others and lead to bad quality meshes. To avoid such situations, we need to adjust the normal direction of these vertices by taking the average of their neighboring normals.

4 Fluid-Structure Interaction Simulation

The blood flow is governed by the incompressible Navier-Stokes equations posed on a moving domain. The Arbitrary Lagrangian-Eulerian (ALE) formulation is used, which is a popular approach for vascular blood flow applications. The ar-

terial wall is modeled as a three-dimensional isotropic hyperelastic solid in the Lagrangian description. At the interface between the blood and the elastic wall, velocity and traction compatibility conditions are assumed to hold. The motion of the fluid domain is governed by the equations of linear elasticity subject to displacement boundary conditions coming from the motion of the arterial wall. The density, and dynamic viscosity of the fluid are 1 g/cm^3 and 0.04 $g/(cm \cdot s)$, respectively. The density, Young's modulus, and Poisson's ratio of the arterial wall in the reference configuration are 1 g/cm^3, $10^7 dyn/cm^2$, and 0.45, respectively. The arterial wall thickness is taken to be approximately 0.018 cm. Pulsatile velocity is applied at the inlet branch and resistance boundary conditions are set at the outlet branches. The resistance boundary conditions are posed such that physiological pressure levels are attained in the simulations.

The discretization for both the fluid and solid consists of linear tetrahedral elements. The meshes for the fluid and solid are compatible at the interface. The discrete fluid formulation makes use of the recently proposed residual-based variational multiscale method [Bazilevs, Calo, Cottrel, Hughes, Reali, and Scovazzi (2007)]. The solid and fluid mesh motion equations are discretized using the Galerkin approach. The time-dependent equations are solved using the generalized-time integrator developed for fluid-structure interaction in [Bazilevs, Calo, Hughes, and Zhang (2008)]. A monolithic solution strategy is adopted in which the increments of the fluid and solid variables are obtained in a simultaneous fashion (see [Bazilevs, Calo, Zhang, and Hughes (2006)], [Bazilevs, Calo, Hughes, and Zhang (2008)] for details). The effect of the mesh motion on the fluid equations is omitted from the tangent matrix for efficiency, as advocated in [Bazilevs, Gohean, Hughes, Moser, and Zhang (2009)].

5 Results and Discussion

We apply our meshing techniques to four cerebral aneurysm models. From the CTA RAW imaging data, we construct tetrahedral meshes using the octree-based isocontouring method. Then we utilize the edge contraction to remove non-manifold situations. After pillowing, the optimization-based smoothing is used to improve the minimum volume of the mesh, and then geometric flow smoothing is adopt to improve the overall quality of the mesh. Three planes are defined to cut the aneurysms, and the geometric flow is used again to improve the quality near the cutting plane. After that, the fluid volume is of good quality, and boundary layers are constructed for the solid part of the aneurysms. The final meshes of the four models are presented in Figs. 5-8, and Fig. 4 shows the histogram of the edge-ratio, Joe-Liu parameter, and volume. Tab. 1 lists the best/worst edge ratio, the best/worst Joe-Liu parameter, and the minimal/maximal volume for the four models.

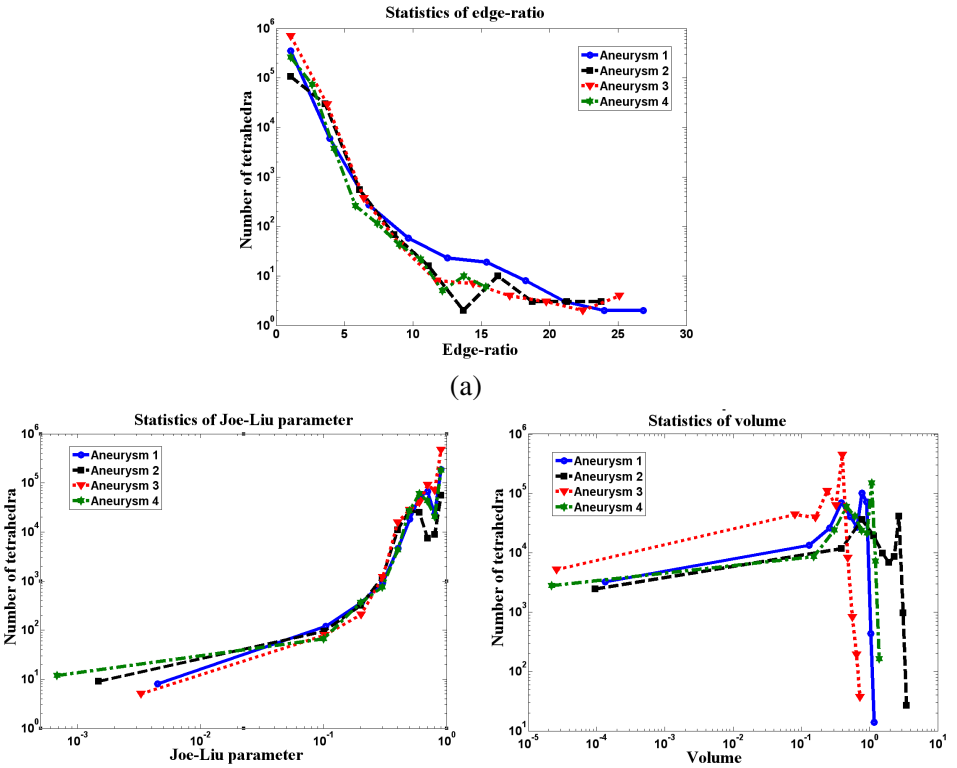

Figure 4: The histogram of (a) the edge-ratio, (b) the Joe-Liu parameter, and (c) the element volume of four aneurysm models.

Table 1: The three quality criteria of four aneurysm models.

	Vertex Number	Tetra Number	Edge-ratio (best, worst)	Joe-Liu parameter (best, worst)	Volume (min, max)
Model 1	64029	354114	(1.05, 29.72)	$(1.0, 4.48 \times 10^{-3})$	$(1.35 \times 10^{-4}, 1.30)$
Model 2	25116	136881	(1.06, 26.30)	$(1.0, 1.48 \times 10^{-3})$	$(9.50 \times 10^{-5}, 3.86)$
Model 3	125874	719193	(1.05, 27.77)	$(1.0, 3.28 \times 10^{-3})$	$(2.60 \times 10^{-5}, 0.80)$
Model 4	60933	338419	(1.06, 16.90)	$(1.0, 6.82 \times 10^{-4})$	$(2.20 \times 10^{-5}, 1.53)$

The constructed meshes are employed in the fluid-structure interaction simulations. Fig. 5(c) and Figs. 6-8(b) show blood flow streamlines at the peak systole for Models 1, 2, 3, and 4. The flow appears to be complex with several vortical features present, yet not turbulent. Fig. 5(d) and Figs. 6-8(c) show the blood vessel shear stress at the fluid-solid interface. The wall shear stress tends to arrive at the max-

imum near the region where the jet of blood coming from the inflow impinges on the aneurysm wall. Fig. 5(b) shows the displacement configuration of Aneurysm 1 incurred during the cycle.

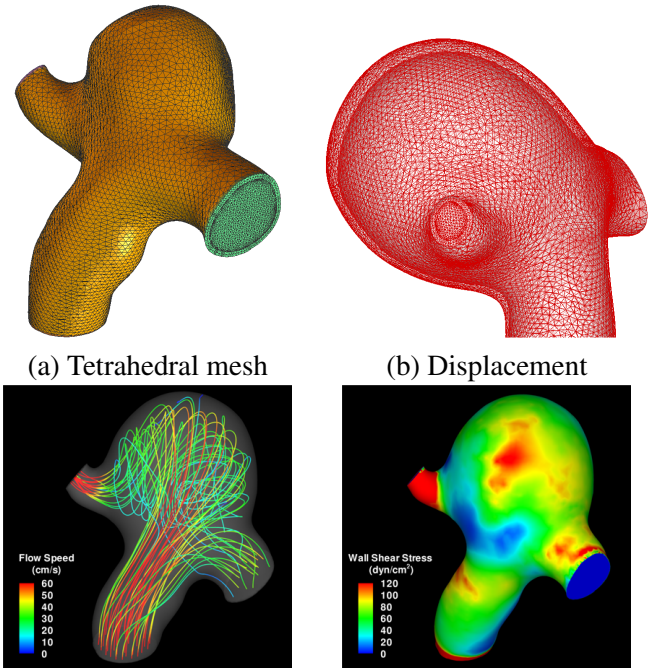

(a) Tetrahedral mesh (b) Displacement

(c) Velocity streamlines (d) Wall shear stress

Figure 5: The constructed mesh with boundary layer and the simulation results for Aneurysm 1.

6 Conclusion and Future Work

In this paper, we have developed a comprehensive approach to generate high-fidelity finite element meshes for the FSI simulation of cerebral aneurysms. A series of techniques are applied to obtain these high quality meshes, including image processing, mesh generation, quality improvement, plane cutting, and boundary layer generation. Fluid-structure interaction analysis predicts arterial wall displacement that is in good agreement with that reported by other researchers and observed in practice. Flow streamlines suggest that the flow is unsteady and complex, yet not turbulent. The wall shear stress distribution is also very reasonable. Uniform thickness is used in our mesh generation procedure. In the future, we can

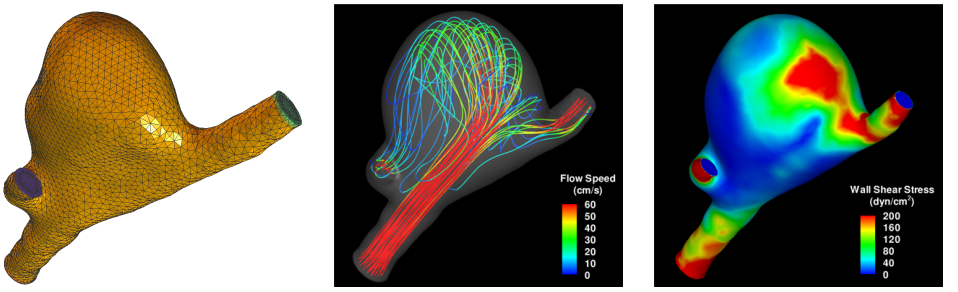

(a) Tetrahedral mesh (b) Velocity streamlines (c) Wall shear stress

Figure 6: The constructed mesh with boundary layer and the simulation results for Aneurysm 2.

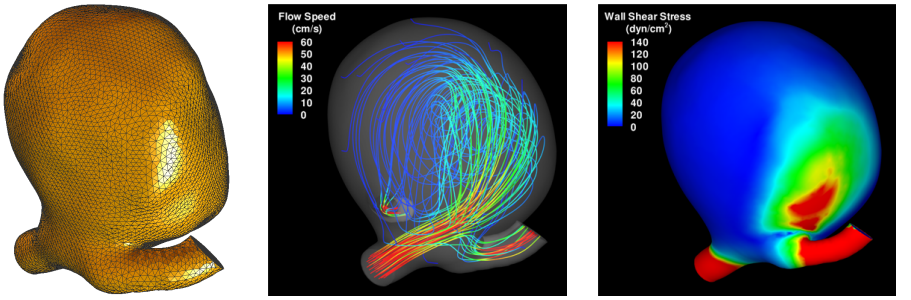

(a) Tetrahedral mesh (b) Velocity streamlines (c) Wall shear stress

Figure 7: The constructed mesh with boundary layer and the simulation results for Aneurysm 3.

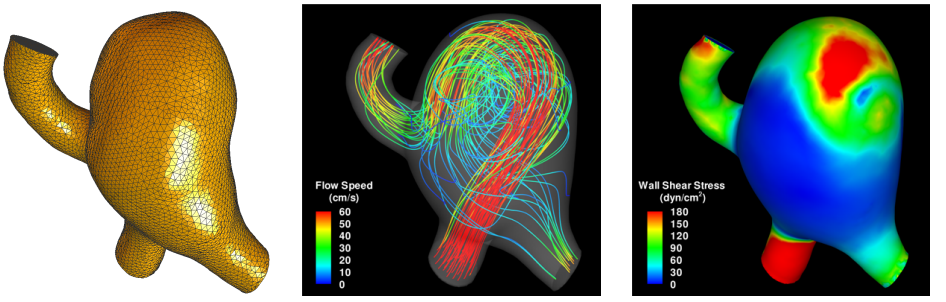

(a) Tetrahedral mesh (b) Velocity streamlines (c) Wall shear stress

Figure 8: The constructed mesh with boundary layer and the simulation results for Aneurysm 4.

construct one thickness function according to the simulation results, instead of using uniform thickness. In this way, we include the feedback from simulation results to adjust the geometric model to increase the computational accuracy. In addition, we will work on 20 new aneurysm models, and extract statistic information from them to predict the risk for aneurysm rupture.

Acknowledgement: An early version of this paper was published in International Conference on Computational & Experimental Engineering and Sciences 2009 [Zhang, Wang, Liang, Bazilevs, Hsu, Kvamsdal, Brekken, and Isaksen (2009)]. This research was supported in part by a gift fund from SINTEF ICT, Norway.

References

Bazilevs, Y.; Calo, V.; Cottrel, J.; Hughes, T.; Reali, A.; Scovazzi, G. (2007): Variational multiscale residual-based turbulence modeling for large eddy simulation of incompressible flows. *Computer Methods in Applied Mechanics and Engineering*, vol. 197, pp. 173–201.

Bazilevs, Y.; Calo, V.; Hughes, T. J.; Zhang, Y. (2008): Isogeometric fluid-structure interaction: theory, algorithms, and computations. *Computational Mechanics*, vol. 43, pp. 3–37.

Bazilevs, Y.; Calo, V.; Zhang, Y.; Hughes, T. J. (2006): Isogeometric fluid-structure interaction analysis with applications to arterial blood flow. *Computational Mechanics*, vol. 38, pp. 310–322.

Bazilevs, Y.; Gohean, J.; Hughes, T.; Moser, R.; Zhang, Y. (2009): Patient-specific isogeometric fluid-structure interaction analysis of thoracic aortic blood flow due to implantation of the Jarvik 2000 left ventricular assist device. *Computer Methods in Applied Mechanics and Engineering*. In press.

Canann, P. A.; Tristano, J. R.; Staten, M. L. (1998): An approach to combined Laplacian and optimization-based smoothing for triangular, quadrilateral and quad-dominant meshes. In *7th International Meshing Roundtable*, pp. 479–494.

Charalambous, C.; Conn, A. (1978): An efficient method to solve the minimax problem directly. *SIAM Journal of Numerical Analysis*, vol. 15, no. 1, pp. 162–187.

Chen, L. (2002): Phase-field models for microstructure evolution. *Annual Review of Materials Research*, vol. 32, pp. 113–140.

Cheng, S.-W.; Dey, T. K. (2002): Quality meshing with weighted Delaunay refinement. In *Proc. 13th ACM-SIAM Sympos. Discrete Algorithms (SODA)*, pp. 137–146.

Cheng, S.-W.; Dey, T. K.; Edelsbrunner, H.; Facello, M. A.; Teng, S. (2000): Sliver exudation. *Proc. Journal of ACM*, vol. 47, pp. 883–904.

Chew, L. P. (1997): Guaranteed-quality Delaunay meshing in 3D (short version). In *13th ACM Symposium on Computational Geometry*, pp. 391–393.

Farhat, C.; Geuzaine, P. (2004): Design and analysis of robust ALE time-integrators for the solution of unsteady flow problems on moving grids. *Computer Methods in Applied Mechanics and Engineering*, vol. 193, pp. 4073–4095.

Field, D. A. (1988): Laplacian smoothing and Delaunay triangulations. *Communications in Applied Numerical Methods*, vol. 4, pp. 709–712.

Figueroa, A.; Vignon-Clementel, I.; Jansen, K.; Hughes, T.; Taylor, C. (2006): A coupled momentum method for modeling blood flow in three-dimensional deformable arteries. *Computer Methods in Applied Mechanics and Engineering*, vol. 195, pp. 5685–5706.

Formaggia, L.; Gerbeau, J.-F.; Nobile, F.; Quarteroni, A. (2001): On the coupling of 3D and 1D Navier-Stokes equations for flow problems in compliant vessels. *Computer Methods in Applied Mechanics and Engineering*, vol. 191, pp. 561–582.

Fujishiro, I.; Y. Maeda, H. S.; Takeshima, Y. (1996): Volumetric data exploration using interval volume. *IEEE Transactions on Visualization and Computer Graphics*, vol. 2, no. 2, pp. 144–155.

George, P. L.; Borouchaki, H. (1998): *Delaunay triangulation and meshing, application to finite elements*. Hermes, Paris, France.

Glimm, J.; Grove, J.; Li, X.; Tan, D. (2000): Robust computational algorithms for dynamic interface tracking in three dimensions. *SIAM Journal on Scientific Computing*, vol. 21, pp. 2240–2256.

Goncalves, P.; Tavares, J.; Jorge, R. (2008): Segmentation and simulation of objects represented in images using physical principles. *CMES: Computer Modeling in Engineering & Sciences*, vol. 32, no. 1, pp. 45–55.

Hansbo, P. (1995): Generalized Laplacian smoothing of unstructured grids. *Communications in Numerical Methods in Engineering*, vol. 11, pp. 455–464.

Harvie, D.; Fletcher, D. (2000): A new volume of fluid advection algorithm: the stream scheme. *Journal of Computational Physics*, vol. 162, pp. 1–32.

Isaksen, J.; Bazilevs, Y.; Kvamsdal, T.; Zhang, Y.; Kaspersen, J.; Waterloo, K.; Romner, B.; Ingebrigtsen, T. (2008): Determination of wall tension in cerebral artery aneurysms by numerical simulation. *Stroke*, vol. 39, pp. 3172–3178.

Isaksen, J.; Egge, A.; Waterloo, K.; Romner, B.; Ingebrigtsen, T. (2002): Risk factors for aneurysmal subarachnoidal haemorrhage: the tromsø study. *Journal of Neurology, Neurosurgery Psychiatry*, vol. 73, pp. 185–187.

Liu, A.; Joe, B. (1994): Relationship between tetrahedron shape measures. *BIT*, vol. 34(2), pp. 268–287.

Liu, W.; Liu, Y.; Farrell, D.; Zhang, L.; Wang, X.; Fukui, Y.; Patankar, N.; Zhang, Y.; Bajaj, C. L.; Lee, J.; Hong, J.; Chen, X.; Hsu, H. (2006): Immersed finite element method and its applications to biological systems. *Computer Methods in Applied Mechanics and Engineering*, vol. 195, no. 13-16, pp. 1722–1749.

Lohner, R.; Parikh, P. (1988): Three dimensional grid generation by the advancing front method. *International Journal for Numerical Methods in Fluids*, vol. 8, pp. 1135–1149.

Lorensen, W. E.; Cline, H. E. (1987): Marching cubes: A high resolution 3D surface construction algorithm. In *Proceedings of SIGGRAPH*, pp. 163–169.

Meyer, M.; Desbrun, M.; Schroder, P.; Burr, A. H. (2002): *Discrete differential-geometry operators for triangulated 2-manifolds*. Springer-Verlag.

Nielson, G. M.; Sung, J. (1997): Interval volume tetrahedrization. In *IEEE Visualization*, pp. 221–228.

Osher, S.; Fedkiw, R. (2003): *Level set methods and dynamic implicit surfaces*. Springer, Berlin.

Owen, S. (1998): A survey of unstructured mesh generation technology. In *7th International Meshing Roundtable*, pp. 26–28.

Rider, W.; Kothe, D. (1995): A marker particle method for interface tracking. In *Proceedings of 6th International Symposium on Computational Fluid Dynamics*, pg. 976.

Rinkel, G.; Djibuti, M.; Algra, A. (1998): Prevalence and risk of rupture of intracranial aneurysms: a systematic review. *Stroke*, vol. 29, pp. 251–256.

Sethian, J. (1999): *Level set methods and fast marching methods*. Cambridge University Press, Cambridge.

Shephard, M. S.; Georges, M. K. (1991): Three-dimensional mesh generation by finite octree technique. *International Journal for Numerical Methods in Engineering*, vol. 32, pp. 709–749.

Shewchuk, J. R. (2002): Constrained Delaunay tetrahedrizations and provably good boundary recovery. In *11th International Meshing Roundtable*, pp. 193–204.

Taylor, C.; Hughes, T.; Zarins, C. (1998): Finite element modeling of blood flow in arteries. *Computer Methods in Applied Mechanics and Engineering*, vol. 158, pp. 155–196.

Tezduyar, T. (2003): Computation of moving boundaries and interfaces and stabilization parameters. *International Journal for Numerical Methods in Fluids*, vol. 43, pp. 555–575.

Torii, R.; Oshima, M.; Kobayashi, T.; Takagi, K.; Tezduyar, T. (2006): Computer modeling of cardiovascular fluid-structure interactions with the deforming-spatial-domain/stabilized space-time formulation. *Computer Methods in Applied Mechanics and Engineering*, vol. 195, pp. 1885–1895.

Uiije, H.; Tamano, Y.; Sasaki, K.; Hori, T. (2001): Is the aspect ratio a reliable index for predicting the rupture of a saccular aneurysm? *Neurosurgery*, vol. 48, pp. 495–502.

Xu, G.; Pan, Q.; Bajaj, C. (2003): *Discrete surface modeling using geometric flows*. Technical Report TR-03-36, Department of Computer Sciences, University of Texas at Austin.

Yang, C.; Tang, D.; Yuan, C.; Kerwin, W.; Liu, F.; Canton, G.; Hatsukami, T.; Atluri, S. (2008): Meshless generalized finite difference method and human carotid atherosclerotic plaque progression simulation using multi-year MRI patient-tracking data. *CMES: Computer Modeling in Engineering & Sciences*, vol. 28, no. 2, pp. 95–107.

Yushkevich, P.; Piven, J.; Hazlett, H.; Smith, R.; Ho, S.; Gee, J.; Gerig, G. (2006): User-guided 3D active contour segmentation of anatomical structures: significantly improved efficiency and reliability. *Neuroimage*, vol. 31, no. 3, pp. 1116–28.

Zhang, Y.; Bajaj, C.; Sohn, B. S. (2005): 3D finite element meshing from imaging data. *Computer Methods in Applied Mechanics and Engineering*, vol. 194, pp. 5083–5106.

Zhang, Y.; Cheng, B.; Oh, C.; Spehar, J.; Burgess, J. (2008): Kinematic analysis of lumbar spine undergoing extension and dynamic neural foramina cross section measurement. *CMES: Computer Modeling in Engineering & Sciences*, vol. 29, no. 2, pp. 55–62.

Zhang, Y.; Wang, W.; Liang, X.; Bazilevs, Y.; Hsu, M.; Kvamsdal, T.; Brekken, R.; Isaksen, J. (2009): High-fidelity tetrahedral meshing from imaging data for fluid-structure interaction analysis of aneurysms. In *International Conference on Computational & Experimental Engineering and Sciences*.

Zhang, Y.; Xu, G.; Bajaj, C. (2006): Quality meshing of implicit solvation models of biomolecular structures. *Computer Aided Geometric Design*, vol. 23, no. 6, pp. 510–530.

Zhou, Y.; Chen, B.; Kaufman, A. (1997): Multiresolution tetrahedral framework for visualizing regular volume data. In *IEEE Visualization*, pp. 135–142.